Shock-induced dust ignition in curved pipeline with steady flow

I. Semenov[a,*], S. Frolov[b], V. Markov[c], P. Utkin[a]

[a]*Institute for Computer Aided Design, RAS, 19/18, 2nd Brestskaya str., 123056, Moscow, Russia*
[b]*Semenov Institute of Chemical Physics, RAS, 4, Kosygina str., 117334, Moscow, Russia*
[c]*V.A. Steklov Mathematical Institute, RAS, 8, Gubkina str., 119991, Moscow, Russia*

Abstract

The ultimate objective of the research outlined in this paper is to determine the conditions governing shock-induced ignition of dusty flows in curved pipelines using analytical and computational approaches. The results of numerical simulation indicate that ignition of two-phase flows in curved channels is mainly conditioned by the shock-induced flow and is not very sensitive to the flow structure in front of the shock wave. The calculations of nonreactive shock propagation in the quasi-steady two-phase flow and in the uniform quiescent dust suspension revealed significant differences in the postshock flow structure downstream the channel corner. Nevertheless, ignition occurred in the region where the predominant role was played by reflected shock waves, i.e., in the vicinity to the channel corner. The results call for further studies dealing with shock-induced ignition and explosion build-up in curved channels.

Introduction

An explosion hazard of pneumatic dust conveyors is the issue of considerable concern for process industries (Bartknecht, 1987; Eckhoff, 1997). In case of accidental ignition of dust suspensions in feeders, cyclones, separators, filters, or other equipment attached to the dust conveyors, severe local explosions can occur and a danger of explosion transmission to other processing units through the conveyor manifolds exists. Physical mechanisms of explosion transmission and accident escalation include a possibility of flame propagation in the dust suspension and shock-induced ignition of a dusty flow leading to Deflagration-to-Detonation transition (DDT). The latter scenario is known to be most devastating.

Explosion hazards caused by flame propagation in the pneumatic dust conveyors were studied both experimentally and theoretically elsewhere (Bartknecht, 1987; Eckhoff, 1997; Vogl, 1996; Bielert & Sichel, 1997). The flame propagation velocity was shown to depend on many parameters including dust type and concentration in the flow, flow velocity, tube diameter and length, ignition location and ignition source, etc. Moreover, experiments of full-scale dust conveying systems under realistic operating conditions were performed.

Shock-induced ignition and detonation of reactive dust suspensions was studied for simple initial configurations. Among them (*i*) quiescent dust suspensions in channels of constant or variable cross-section (e.g., Korobeinikov, 1993; Kutushev & Shorohova, 2002), (*ii*) confined dust clouds with well defined boundaries (e.g., Fedorov & Khmel, 2002), (*iii*) infinite-length, thin, dense dust layers (e.g., Kauffman, Sichel & Wolanski, 1992; Korobeinikov, Semenov, Men'shov, Klemens, Wolanski & Kosinski, 2002), and (*iv*) finite-length, thin, dense dust layers with a definite shape of the upwind edge (e.g. Fedorov & Fedorchenko, 2005). On the one hand, such studies revealed salient features of shock-induced

* Corresponding author. Tel.: +7 495 2508286; fax: +7 495 2509554.
E-mail address: semenov@icad.org.ru

ignition processes and provided useful information on characteristic time and length scales inherent in the ignition phenomenon. On the other hand, the dust cloud or dense layer formation process, which has a strong influence on the dynamics of dust explosion, is out of consideration in such studies. The ultimate objective of the research outlined in this paper is to determine the conditions governing shock-induced ignition of dusty flows in curved pipelines using analytical and computational approaches. It is implied that this study will provide information on possible similarity conditions for modeling large-scale explosions in pipelines using laboratory-scale installations.

1. Problem Formulation

1.1 Flow configuration

As the starting point of the research, the flow configuration shown in Fig. 1 was considered. A gas uniformly laden with monodispersed spherical dust particles of diameter d entered at an inlet velocity U_{in} a curved planar channel of width H and total length L with the 90-degree corner. The lengths of the vertical and horizontal portions of the channel along its central section were L_1 and L_2, respectively, so that $L = L_1 + L_2$. The loading of the flow with the dust at the inlet of the channel was η. It was expected that the steady-state (or quasi-steady-state) flow pattern in the channel could exhibit pronounced stagnation and recirculation zones with dust particles accumulation, as shown schematically in Fig. 1. A shock wave, formed presumably due to accidental explosion outside the channel, could enter the channel either from the inlet or from the outlet. Depending on the incident shock wave strength and compression phase duration, ignition of dust particles could occur either in the free stream or due to complex interaction of the shock-induced flow with confining walls and dust deposits. The issue addressed in this study was to find out whether the steady-state flow pattern in the channel was important for shock-induced ignition of particle suspension or not. In the latter case, the analysis of the explosion hazards could be greatly simplified due to avoiding the necessity of simulating the steady-state flow pattern in the channel.

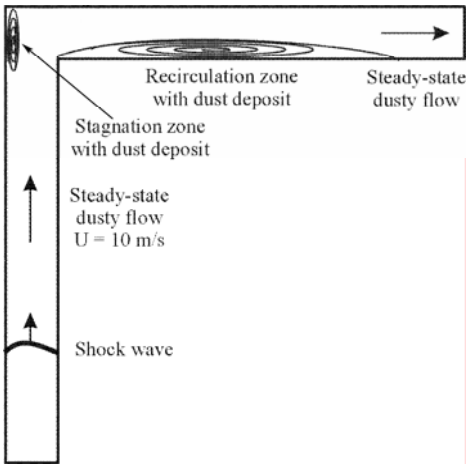

Figure 1: Flow configuration

1.2 Mathematical model

The mathematical statement of the problem was based on two-dimensional equations of two-phase, viscous, reactive, compressible flow within a coupled two-velocity and two-temperature formulation (Nigmatulin, 1987). The set of governing equations is given below:

$$\rho_1 = \sum_{k=1}^{NGSP} \rho_{1,k} \ , \qquad \rho_2 = \sum_{k=1}^{NSSP} \rho_{2,k}$$

$$\partial_t \rho_{1,k} + \partial_m \rho_{1,k} u_{1,m} = -\partial_m J_{k,m} + \tilde{\omega}_{1,k} \ , \qquad k = 1,..,NGSP$$

$$\partial_t \rho_{2,k} + \partial_m \rho_{2,k} u_{2,m} = \tilde{\omega}_{2,k} \ , \qquad k = 1,..,NSSP$$

$$\partial_t (\rho_1 \mathbf{u}_1) + \partial_m (\rho_1 \mathbf{u}_1 u_{1,m}) + \nabla p = -\mathbf{F} - \tilde{\omega}_2 \mathbf{u}_2 + \partial_m \mathbf{T}_m$$

$$\partial_t (\rho_2 \mathbf{u}_2) + \partial_m (\rho_2 \mathbf{u}_2 u_{2,m}) = \mathbf{F} + \tilde{\omega}_2 \mathbf{u}_2$$

$$\partial_t E_1 + \partial_m (E_1 + p) u_{1,m} = -\mathbf{F}\mathbf{u}_2 - Q_T - Q_R - 0.5\tilde{\omega}_2 \mathbf{u}_2^2 - \sum_{l=1}^{NSSP} \tilde{\omega}_{2,l} e_{2,l} -$$

$$-\dot{\omega}_{1,1} Q_v - \dot{\omega}_{2,2} Q_s - \partial_m \left(\sum_{k=1}^{NGSP} h_{1,k} J_{k,m} + \mathbf{q} - \mathbf{T}\mathbf{u}_1 \right)$$

$$\partial_t E_2 + \partial_m E_2 u_{2,m} = \mathbf{F}\mathbf{u}_2 + Q_T + Q_R + 0.5\tilde{\omega}_2 \mathbf{u}_2^2 + \sum_{l=1}^{NSSP} \tilde{\omega}_{2,l} e_{2,l}$$

$$E_1 = 0.5\rho_1 \mathbf{u}_1^2 + \sum_{k=1}^{NGSP} \rho_{1,k} e_{1,k}, \quad E_2 = 0.5\rho_2 \mathbf{u}_2^2 + \sum_{k=1}^{NSSP} \rho_{2,k} e_{2,k}$$

$$e_{1,k} = c_{1,k} T_1 \ , \ k = 1,...,NGSP; \ \ e_{2,k} = c_{2,k} T_2 \ , \ k = 1,...,NSSP$$

$$p = \sum_{k=1}^{NGSP} \rho_{1,k} R_{1,k} T_1 \ , \qquad h_{1,k} = e_{1,k} + R_{1,k} T_1, \ \ k = 1,...,NGSP$$

where t is time, $m=(x, y)$, x and y are the coordinates, ρ is the density, p is the pressure, T is the temperature, c is the specific heat, R is the gas constant, **u** is the velocity vector, **J** is the diffusion mass flux in the gas, $\tilde{\omega}$ is the rate of mass variation, **F** is the interphase force vector, **T** is the stress tensor in the gas, **q** is the heat flux vector in the gas, Q_T and Q_R are the interphase heat fluxes due to convection and radiation, Q_s and Q_v are the chemical energy release by carbon and volatiles oxidation respectively, the NGSP is the number of species in the gas phase, and NSSP is the number of phases in the solid phase. Indices 1 and 2 denote the gas and solid phases, respectively. The interaction between phases was modeled by the standard relationships reported elsewhere (Korobeinikov et al., 2002).

The gas phase was assumed to contain 5 species (*NGSP*=5): CH_4 (k = 1), O_2 (2), N_2 (3), CO_2 (4), and H_2O (k = 5). The dispersed solid-particle phase was assumed to contain 3 species (*NSSP*=3): volatile, CH_4 (k = 1); carbon, C (2), and ash (k = 3). The following chemical reactions are considered:

$$CH_4 + 2O_2 = CO_2 + 2H_2O + Q_{CH_4} \text{ (homogeneous);}$$

$$C + O_2 = CO_2 + Q_C \text{ (heterogeneous)}$$

where Q_{CH_4} =47.9 kJ/g and Q_C = 30 kJ/g. The rates of mass variation for different species was modeled as

$$\tilde{\omega}_{1,1} = \dot{\omega}_{1,1} - \dot{\omega}_{2,1}$$

$$\dot{\omega}_{1,1} = -\rho_{1,2}\rho_{1,1}\sqrt{T_1}B_2 \exp\left(-\frac{E_g}{RT_1}\right),\ E_g = 60 \text{ kJ/mol},\ B_2 = 2.5\cdot 10^{10}\ \text{cm}^3 g^{-1} K^{-1/2} \text{s}^{-1}$$

$$\dot{\omega}_{2,1} = -\rho_{2,1}B_1 \exp\left(-\frac{E_v}{RT_2}\right),\quad E_v = 44 \text{ kJ/mol},\quad B_1 = 2.5\cdot 10^5 \text{s}^{-1}$$

$$\tilde{\omega}_{1,2} = 4\dot{\omega}_{1,1} + \frac{8}{3}\dot{\omega}_{2,2}\ ,\quad \tilde{\omega}_{1,3} = 0\ ,\quad \tilde{\omega}_{1,4} = -\frac{11}{4}\dot{\omega}_{1,1} - \frac{11}{3}\dot{\omega}_{2,2}\ ,\quad \tilde{\omega}_{1,5} = -\frac{9}{4}\dot{\omega}_{1,1}$$

$$\tilde{\omega}_{2,1} = \dot{\omega}_{2,1}$$

$$\tilde{\omega}_{2,2} = \dot{\omega}_{2,2} = -A_s F_s T_1 \rho_{1,2}\rho_{2,2} R_{O_2} \exp\left(-\frac{E_s}{RT_2}\right),\quad R_{O_2} = \frac{R}{\mu_{O_2}}\ ,$$

$$E_s = 144 \text{ kJ/mol},\ A_s = 8.71\cdot 10^3 \text{cm}^{-2} g\ s^{-1} bar^{-1},\ F_s = 4.26\cdot 10^6 \text{cm}^2 g^{-1}$$

1.3 Problem parameters and test cases

Table 1 shows the values of problem parameters used in the calculations. Table 2 shows the test cases studied herein.

Table 1: Problem parameters

Parameters	Value
Initial gas composition:	air
Oxygen	21% (vol.)
Nitrogen	79%(vol.)
Particle composition:	-
Coal	39.1%(wt.)
Ash	6.4%(wt.)
Methane	54.5% (wt.)
Channel width H	0.15 m
Channel length L	4.15 m
Vertical portion length L_1	1.075 m
Horizontal portion length L_2	3.075 m
Initial temperature of gas	293 K
Initial temperature of particles	293 K
Initial pressure	0.1 MPa
Initial particle diameter d_0	50 μm
Particle material density	1300 kg/m^3
Specific heat of particle material	2.2 J/g K
Particle loading η	2 kg/m^3
Inlet velocity U_{in}	10 m/s
Shock wave Mach number M_0	3.0
Computational grid	structured
Number of grid cells along the channel	4000
Number of grid cells across the channel	150

Table 2: Test cases

Case number	Description
Case 1	Steady-state homogeneous airflow
Case 2	Steady-state two-phase flow
Case 3	Shock wave propagation in quasi-steady nonreactive two-phase flow
Case 4	Shock wave propagation in quasi-steady reactive two-phase flow
Case 5	Shock wave propagation in quiescent, uniform, nonreactive dust suspension
Case 6	Shock wave propagation in quiescent, uniform, reactive dust suspension

The first two test cases relate to the steady-state homogeneous (Case 1) and two-phase (Case 2) flow pattern in the channel under consideration. In addition, four test cases with a shock wave entering the channel inlet were studied. In Cases 3 and 4, the shock wave of initial Mach number 3 propagated in the quasi-steady nonreactive (Case 3) and reactive (Case 4) two-phase flow. In Cases 5 and 6, the shock wave of initial Mach number 3 propagated in the quiescent, uniform, nonreactive (Case 5) and reactive (Case 6) dust suspension in air.

1.3 Numerical procedure

The numerical procedure was similar to that reported in (Korobeinikov et al., 2002). It was based on the finite volume approach and Godunov flux approximation and was implemented for parallel computing. The problem was solved at fine (structured) computational grid with 600,000 cells.

2. Results of calculations

2.1 Case 1

The aim of Case 1 was to determine a quasi-steady-state flow pattern in the channel simulating the operation of the pneumatic conveyor without particle loading. The time taken for the flow to attain a quasi-steady state pattern will be denoted as t_s. The boundary conditions were taken as follows:

Inlet:

$$u_{1,x} = 0,\ u_{1,y} = U_{in} = 10 \text{ m/s},\ T_1 = 293 \text{ K},\ \frac{\partial p}{\partial t} - (c_{in} - U_{in})\frac{\partial p}{\partial y} = 0,\ \rho_1 = \rho_1(p, T_1)$$

Outlet:

$$u_{1,x} + X\frac{\partial u_{1,x}}{\partial x} = U_{in},\ \frac{\partial T_1}{\partial x} = \frac{\partial u_{1,y}}{\partial x} = 0,\ \frac{\partial p}{\partial t} + (c_{in} + U_{in})\frac{\partial p}{\partial x} = 0,\ \rho_1 = \rho_1(p, T_1),$$

where X – constant with dimension of length.

Rigid walls:

$$u_{1,x} = u_{1,y} = 0,\ \frac{\partial T_1}{\partial n} = \frac{\partial p}{\partial n} = 0,\ \rho_1 = \rho_1(p, T_1),$$ where n – normal vector to the wall surface

Differential conditions for pressure were taken from (Dorodnitsyn, 2000) to ensure nonreflecting inlet and outlet boundaries required for obtaining a steady-state subsonic flow pattern in the channel.

Figure 2 shows the calculated fields of gas velocity (Fig. 2a) and pressure (Fig. 2b) in the airflow upon the establishment of a quasi-steady flow pattern ($t_s \approx 400$ ms). The flow in the channel exhibits regular velocity and pressure oscillations caused by vortex shedding from the convex corner. The frequency of vortex shedding is about 50-70 Hz. Two distinct recirculation

zones are evident in Fig. 2: one attached to the concave corner and the other behind the convex corner.

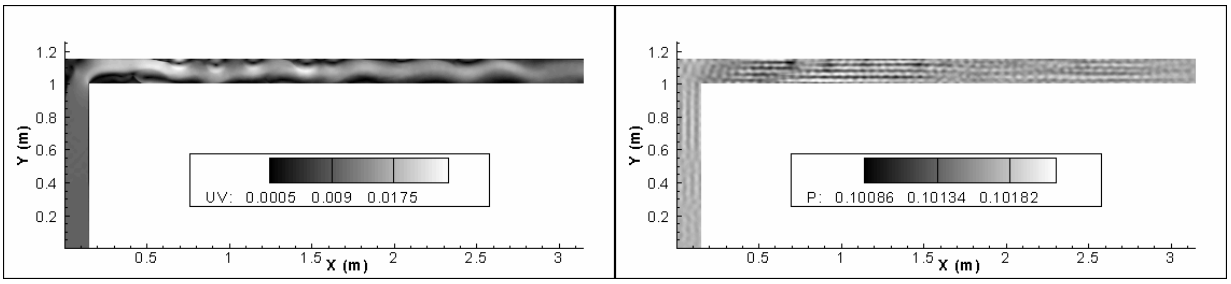

(a) (b)

Figure 2: Predicted fields of (a) gas velocity (in km/s) and (b) pressure (in MPa) in the airflow (Case 1)

2.2 Case 2

The aim of Case 2 was to determine a quasi-steady-state flow pattern in the channel simulating the operation of the pneumatic conveyor with particle loading. Case 2 is the continuation of Case 1 at $t > t_s$. At $t = t_s$, the boundary conditions of Case 1 were supplemented by the conditions for solid particles:

Inlet:

$$u_{2,x} = 0,\ u_{2,y} = U_{in} = 10 \text{ m/s},\ T_2 = 293 \text{ K},\ \rho_2 = 2 \text{ kg/m}^3$$

Outlet:

$$\frac{\partial u_{2,x}}{\partial x} = \frac{\partial u_{2,y}}{\partial x} = \frac{\partial T_2}{\partial x} = \frac{\partial \rho_2}{\partial x} = 0$$

Rigid walls:

$$\mathbf{u}_2 \cdot \mathbf{n} = 0,\ \frac{\partial T_2}{\partial n} = \frac{\partial \rho_2}{\partial n} = 0\text{, where } n \text{ – normal vector to the wall surface}$$

Figure 3 shows the calculated fields of gas velocity (Fig. 3a), pressure (Fig. 3b), particle velocity (Fig. 3c), and particle mass fraction (Fig. 3d) in the two-phase flow, when a quasi-steady flow pattern was established in Case 2. Particles modify considerably the velocity and pressure fields in the channel as follows from the comparison of Figs. 2a and 2b with Figs. 3a and 3b. The vortex shedding frequency decreases to 20–30 Hz and the flow pattern is getting less regular. The most important outcome of Fig. 3 is the existence of pronounced stratification of phases behind the corner. Due to inertia effects, particles hit the upper wall of the channel and move predominantly along this wall for a distance as large as 20*H* (see Fig. 3d). After passing a distance of about 10*H*, particles start entraining into the gas flow in the form of narrow jets hitting the opposite (lower) wall of the channel. The particle entrainment is caused by energetic gas vortices shedding from the convex corner. Despite the entrainment, most of particles are accumulated at the upper wall of the channel.

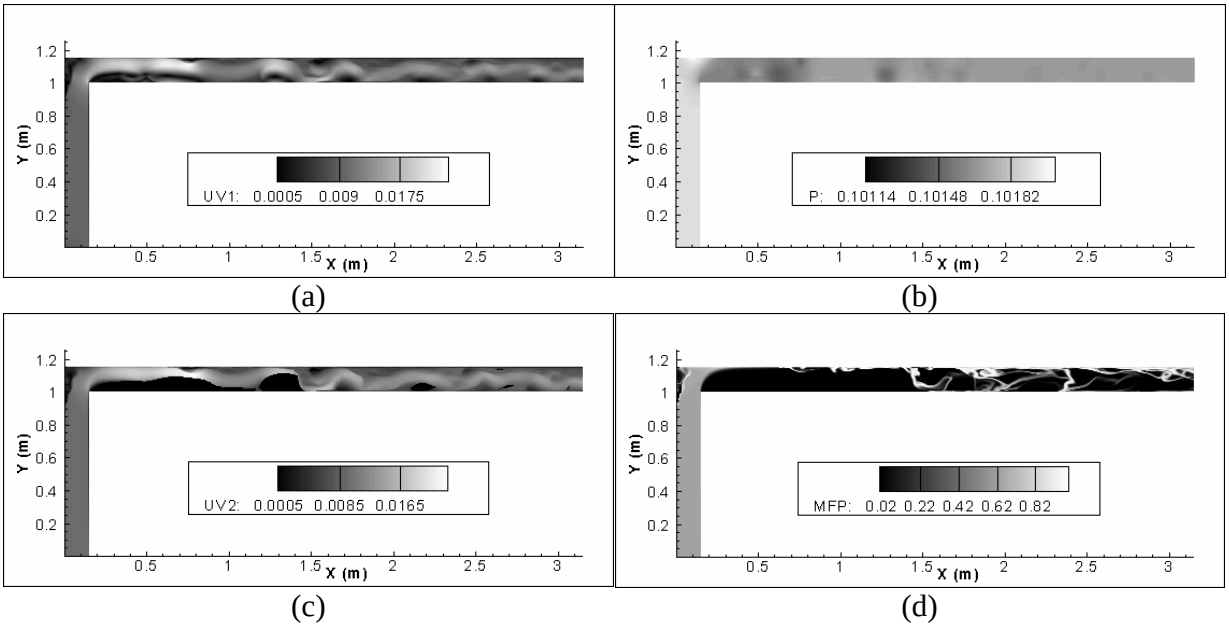

Figure 3: Predicted fields of gas velocity (a), pressure (b), particle velocity (c), and particle mass fraction (d) in the two-phase flow (Case 2)

The pressure traces of Fig. 4 taken at different locations in the channel indicate that the flow is quasi-state indeed.

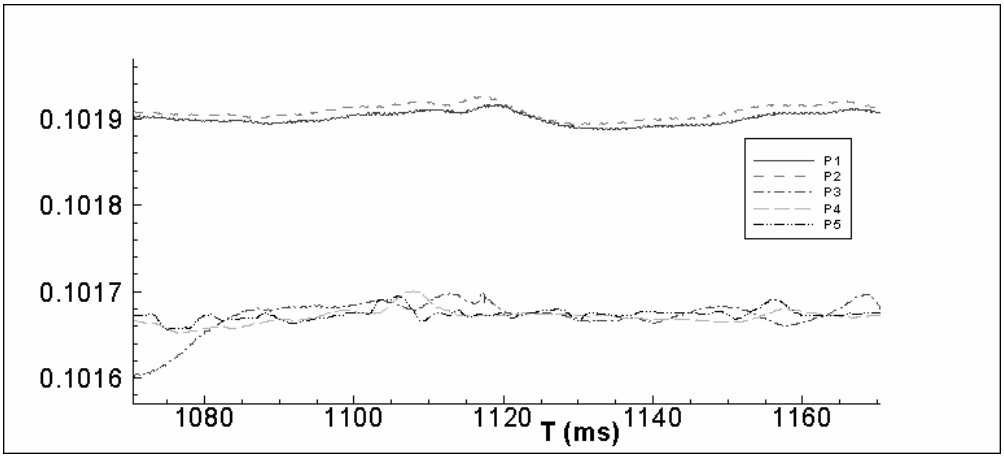

Figure 4: Predicted pressure traces in several channel locations along the symmetry line in Case 2: P1 – at the inlet, P2 – in the middle of the vertical channel arm, P3 – between the convex and concave corners, P4 – in the middle of horizontal channel arm, and P5 – at the outlet.

2.3 Case 3

The aim of Case 3 was to determine the response of the flow pattern of Case 2 to a nonreactive shock wave of initial Mach number $M_0 = 3.0$ entering the channel through the inlet. In view of it, special attention was paid to the inlet boundary conditions. When the flow pattern in Case 2

approached a quasi-steady-state, the boundary conditions at the channel inlet were changed stepwise to ensure the formation of a shock wave in the flow. For this purpose, the pressure, density, gas velocity, and temperature of air at the open boundary were specified according to Rankine-Hugoniot relationships. The duration τ of the shock-induced flow at the inlet boundary was taken finite in order to simulate a shock wave with a finite compression phase. To simplify the solution, it was assumed that during time $\tau = 0.5ms$ only air entered the computational domain through the inlet.

Figure 5 shows the calculated fields of gas velocity (Fig. 5a), pressure (Fig. 5b), particle velocity (Fig. 5c), and particle mass fraction (Fig. 5d) in the nonreactive two-phase flow at the time instant when the shock wave traversed the channel corner and traveled a distance of about 11*H* downstream of it. The shock-induced gas velocity and overpressure are considerably higher than in the undisturbed two-phase flow. Nevertheless, both the 90-degree turn of the channel and the flow structure in front of the propagating shock waves affect the flow pattern behind the shock. Shock reflection from the upper horizontal wall results in the formation of the reflected waves propagating upstream toward the inlet and downstream toward the primary shock diffracted over the convex corner. The former shock wave reverses the flow in the channel. The shock waves propagating downstream exhibit regular reflections from the upper and lower channel walls which induce particle entrainment from the dense layer attached to the upper channel wall into the postshock flow in the form of discrete energetic jets (see Fig. 5d).

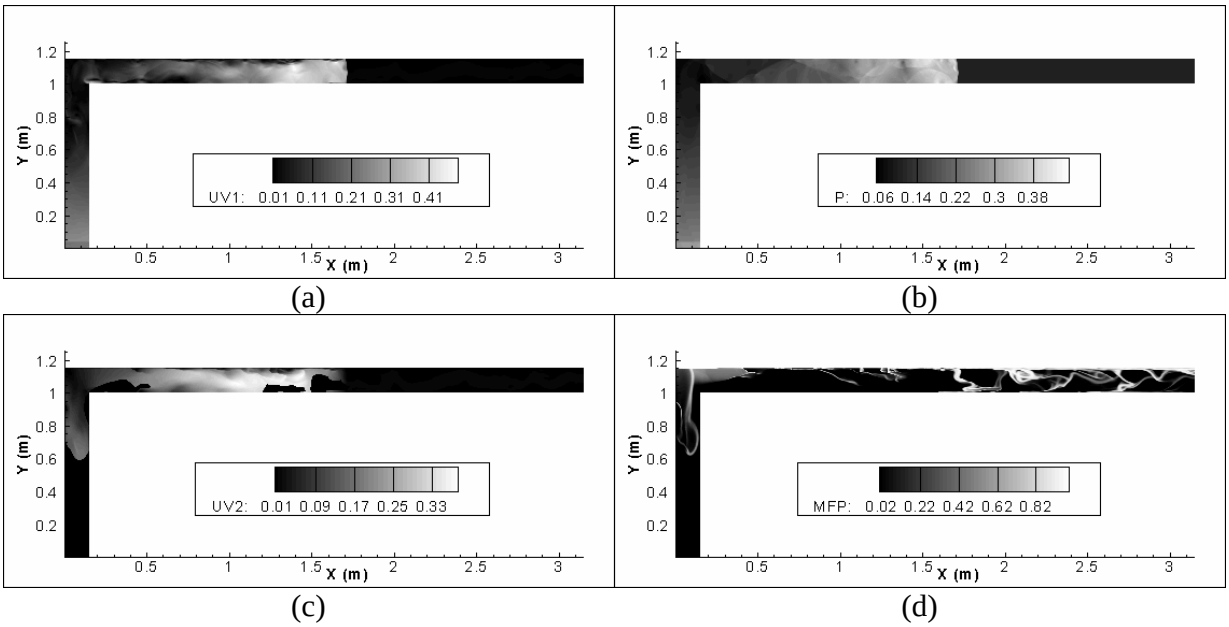

Figure 5: Predicted fields of gas velocity (a), pressure (b), particle velocity (c), and particle mass fraction (d) in the two-phase flow with the nonreactive shock wave (Case 3)

2.4 Case 4

The aim of Case 4 was to determine the response of the flow pattern to a reactive shock wave of initial Mach number M_0 = 3.0 entering the channel through the inlet, and, in particular, to determine the location and conditions of shock-induced ignition in the flow. Figure 6 shows the calculated fields of gas velocity (Fig. 6a), pressure (Fig. 6b), particle velocity (Fig. 6c), particle

mass fraction (Fig. 6d), and temperature of gas (Fig. 6e) in the reactive two-phase flow at the time instant shortly after the shock-induced ignition.

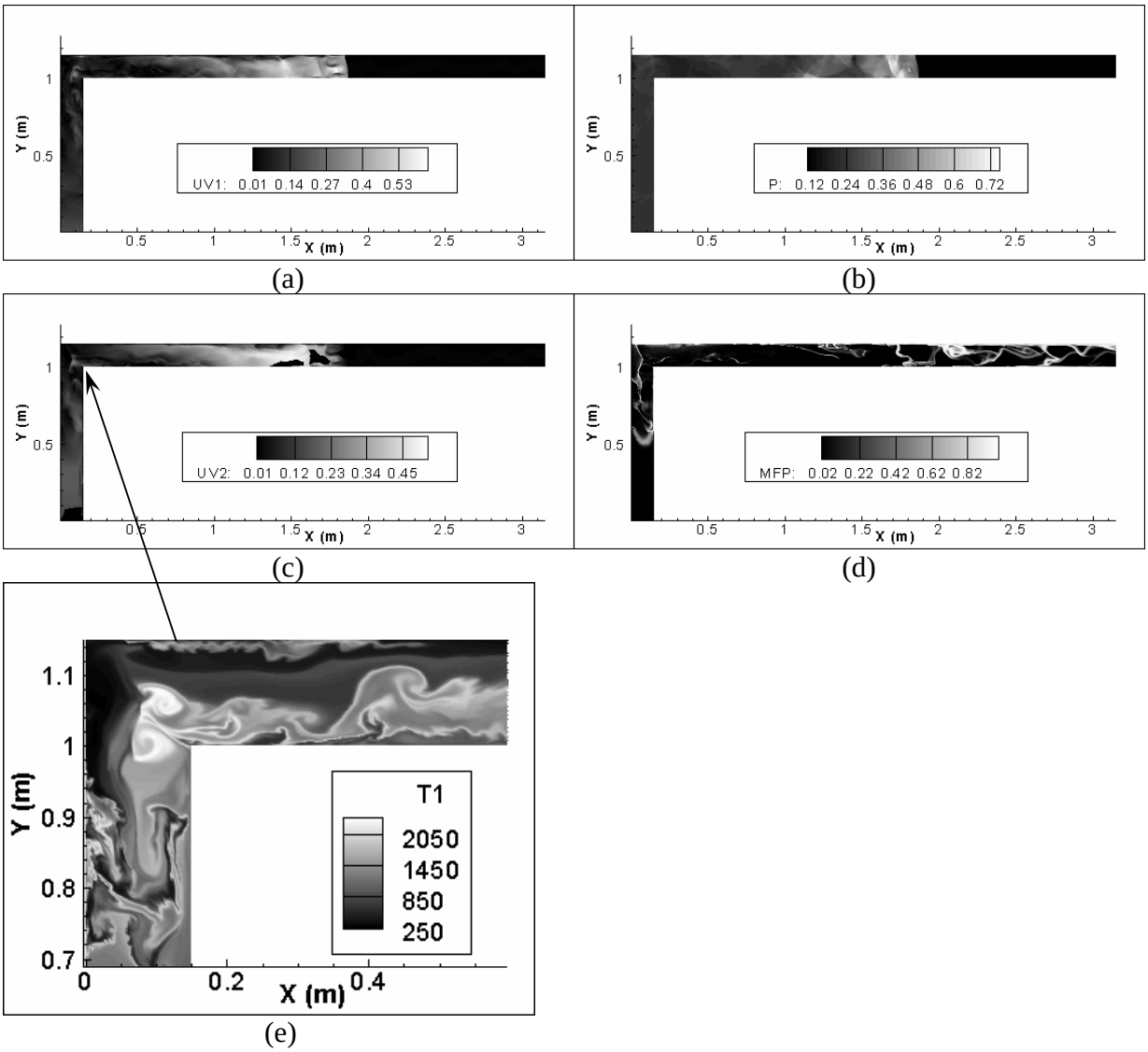

Figure 6: Predicted fields of gas velocity (a), pressure (b), particle velocity (c), particle mass fraction (d), temperature of gas (e), in the reactive two-phase flow (Case 4). Arrow shows the ignition site.

First ignition was found to occur in the corner area in the shear layers formed by interacting incident and reflected shock waves. The flow in this area has a very complex structure shown in the exploded view on Fig. 6e.

2.5 Case 5

In Case 5, the quasi-state flow pattern of Case 2 was replaced by the uniform quiescent suspension of solid particles. The aim of Case 5 was to determine the response of the uniform

dust suspension to a nonreactive shock wave of initial Mach number M_0 = 3.0 entering the channel through the inlet. The shock wave generation technique and parameters were the same as in Case 3.

Figure 7 shows the calculated fields of gas velocity (Fig. 7a), pressure (Fig. 7b), particle velocity (Fig. 7c), and particle mass fraction (Fig. 7d) in the nonreactive, initially quiescent dust suspension at the time instant when the shock wave diffracts over the convex corner and travels a distance of about 10*H*. There are both differences and similarities in the flow patterns of Fig. 7 and Fig. 5. In Case 5, there is a uniform two-phase flow behind a diffracted shock wave, whereas in Case 3 the diffracted shock wave propagates in a highly stratified two-phase flow with particles concentrated at the upper wall. Nevertheless, the diffraction of the primary shock wave in both Cases results in flow stratification behind the convex corner. In Case 5 (see Fig. 7d), similar to Case 3 (see Fig. 5d) the particles involved in motion behind the primary shock wave get collecting near the upper wall of the channel. This effect results in the formation of a flow region behind the convex corner with a very small concentration of particles.

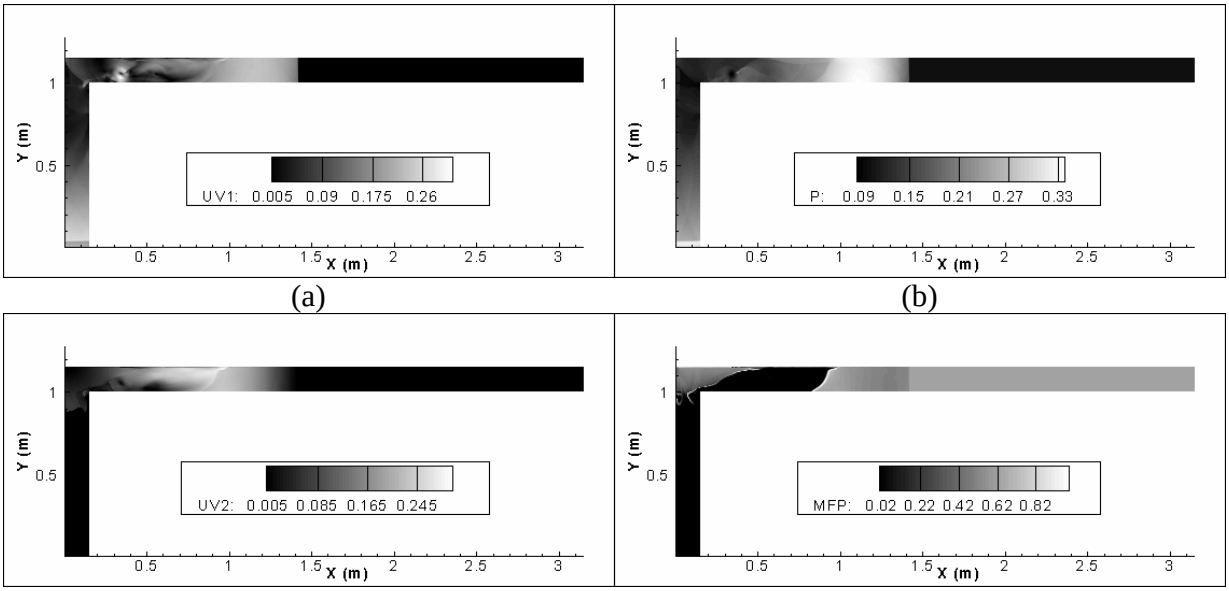

Figure 7: Predicted fields of gas velocity (a), pressure (b), particle velocity (c), and particle mass fraction (d) in the nonreactive, initially uniform dust suspension (Case 5)

2.6 Case 6

The aim of Case 6 was to determine the response of the uniform dust suspension to a nonreactive shock wave of initial Mach number M_0 = 3.0 entering the channel through the inlet and to determine the location and conditions of shock-induced ignition in the flow. Figure 8 shows the calculated fields of gas velocity (Fig. 8a), pressure (Fig. 8b), particle velocity (Fig. 8c), particle mass fraction (Fig. 8d) and temperature of gas (Fig. 8e) in the reactive initially quiescent dust suspension shortly after the time instant when the shock-induced ignition occurred in the region behind the convex corner.

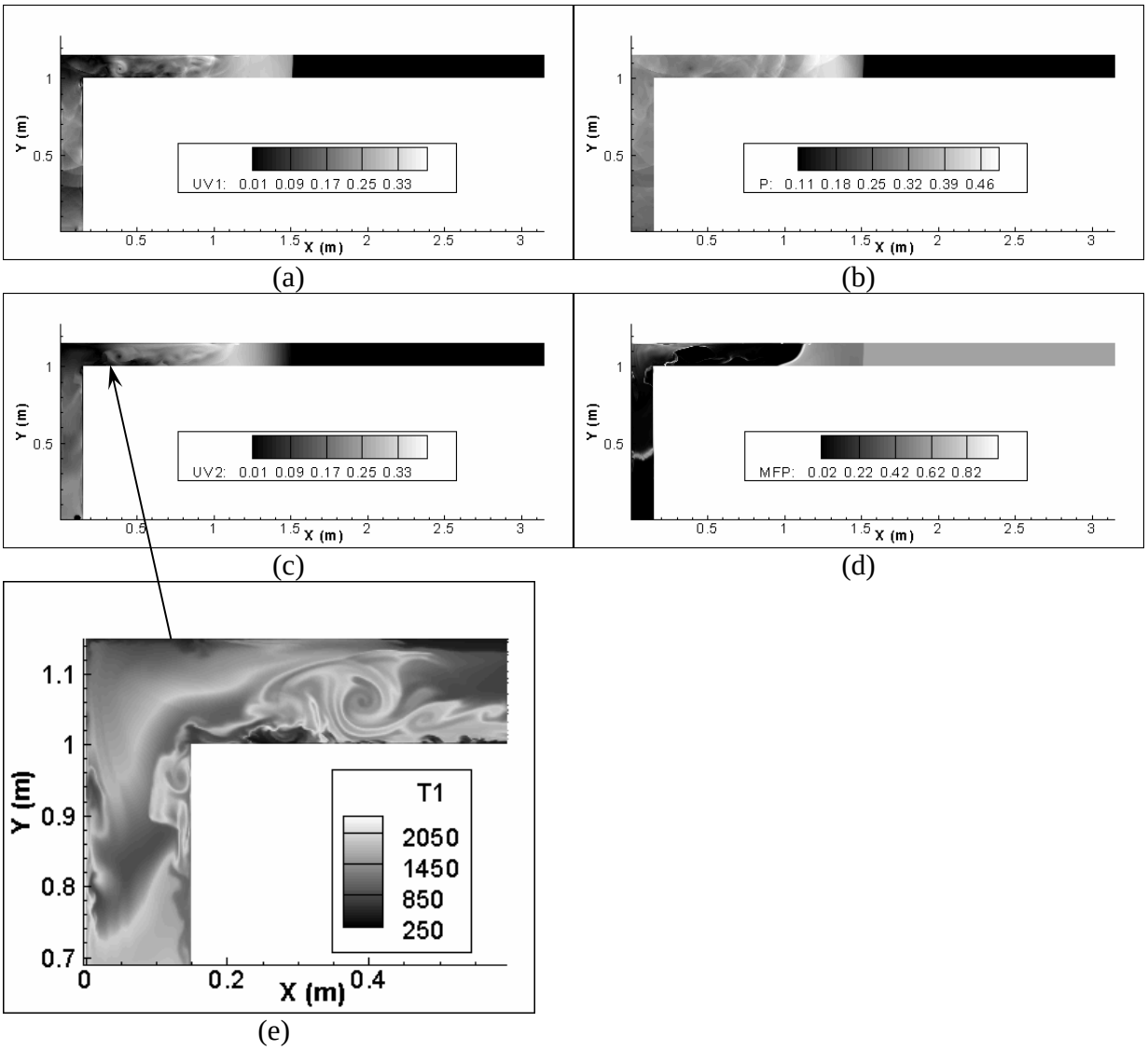

Figure 8: Predicted fields of gas velocity (a), pressure (b), particle velocity (c), particle mass fraction (d) and temperature of gas (e) in the reactive, initially uniform dust suspension (Case 6). Arrow shows the ignition sites.

The ignition was found to occur in the shear layers formed by interacting incident and reflected shock waves (see the exploded view on Fig. 8e). It is important to note that ignition in Cases 4 and 6 occurred at nearly the same time and in nearly the same flow region (near the channel corner) despite significant differences in the flow structure.

3. Discussion and conclusion

Figure 9 shows the comparison of predicted pressure histories in Cases 3 to 6 in the channel cross section connecting the convex and concave corners. Shown in Fig. 9a are the results for nonreactive Cases 3 (upper part) and 5 (lower part). Figure 9b relates to the reactive Cases 4

(upper part) and 6 (lower part). Clearly, the differences in the corresponding pressure histories are insignificant both qualitatively and quantitatively.

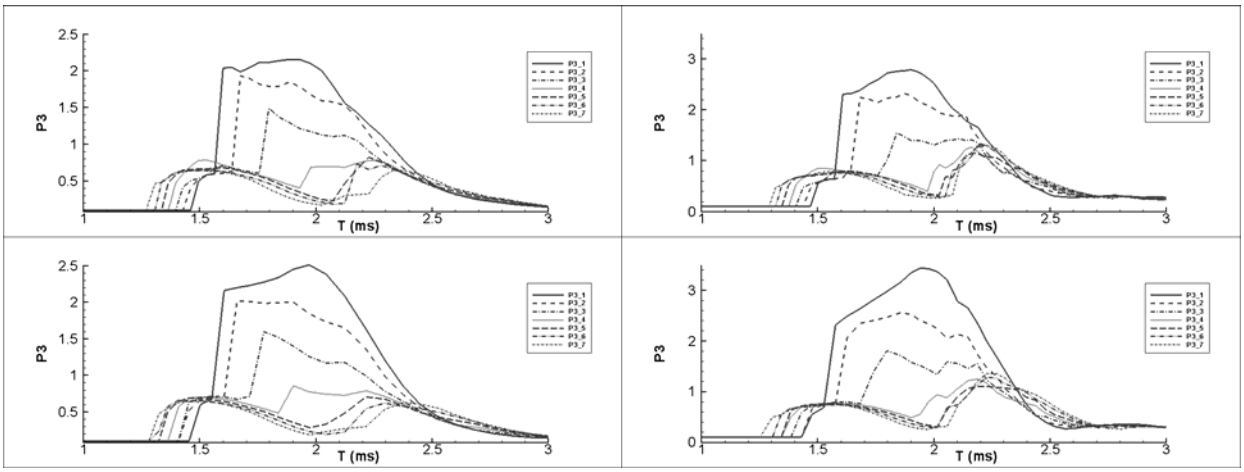

(a) (b)

Figure 9: Comparison of predicted pressure histories in Cases 3 to 6 in the channel cross-section connecting the convex and concave corners. (a) nonreacting dust (upper part – Case 3, lower part – Case 5), (b) reactive dust (upper part – Case 4, lower part – Case 6). Pressure monitoring locations P3_1 to P3_7 are distributed equidistantly along the cross-section with P3_1 located at a distance of 22 mm from the concave corner.

Thus, the results of calculations indicate that ignition of two-phase flows in curved channels is mainly conditioned by the shock-induced flow and is not very sensitive to the flow structure in front of the shock wave. The calculations of nonreactive shock propagation in the quasi-steady two-phase flow and in the uniform quiescent dust suspension revealed significant differences in the postshock flow structure downstream the channel corner. Nevertheless, ignition occurred in the region where the predominant role was played by reflected shock waves, i.e., in the vicinity to the channel corner.

There are two important implications of the results obtained. Remind that the calculations were performed for the shock waves of rather high intensity (Mach 3). Dust ignition in weaker primary shock waves could be affected by the flow structure in the channel. Also, the calculations were focused on dust ignition rather than subsequent flame propagation and explosion build-up. The flow structure could exert a strong influence on the explosion dynamics in the channel.

Acknowledgments

This work is supported by the Russian Foundation for Basic Research (grants 05-08-18200 and 05-08-50115). Dr. I. Semenov also acknowledges the support of "Russian Science Support Foundation".

References

1. Bartknecht, W. (1987). *Staubexplosionen – Ablauf und Schutzmassnahmen.* Springer Verlag, Heidelberg.
2. Eckhoff, R.K. (1997). *Dust explosions in the process industries* (2nd ed.). Oxford: Butterworth-Heinemann.

3. Vogl, A. (1996). *Flame propagation in tubes of pneumatic conveying systems and exhaust equipment. Proc. 29th Loss Prevention Symposium. New Orleans.*
4. Bielert, U., Sichel, M. (1997). *Numerical simulation of dust explosions in pneumatic conveyors. Proc. 16th Colloq. (Intern.) Dynamics of Explosions and Reactive Systems*, Univ. Mining and Metallurgy, Cracow, Poland, p. 99-101.
5. Korobeinikov, V.P. (1993). *The analysis of basic parameters for detonation of dusty gases. Proc. 5th Colloq. (Intern.) Dust Explosions*, Pultusk, Poland, pp. 351-364.
6. Kutushev, A.G., Shorohova, L.V. (2002). *Numerical investigation of burning and detonation of monofuel suspensions in sharply extending tubes.* In: Advances in Confined Detonations. Ed. by Roy G., Frolov S., Santoro R., and Tsyganov S. Moscow, Torus Press, pp. 161-166.
7. Fedorov, A.V., Khmel, T.A. (2002). *Formation of two-dimensional detonation structure in aluminum gas suspension in a channel.* In: Advances in Confined Detonations. Ed. by Roy G., Frolov S., Santoro R., and Tsyganov S. Moscow, Torus Press, pp. 144-149.
8. Kauffman, C.W., Sichel, M., Wolanski, P. (1992). Research on dust explosions at the University of Michigan. Powder Technology, 71, p. 188.
9. Korobeinikov, V.P., Semenov, I.V., Men'shov, I.S., Klemens, R., Wolanski, P., Kosinski, P. (2002). Modelling of flow and combustion behind shock waves propagating along dust layers in long ducts. *Journal of Physics (IV France), 12*, Pr7-113—Pr7-119.
10. Fedorov, A.V., Fedorchenko I.A. (2005) Computation of Dust Lifting behind a Shock Wave Sliding along the Layer. Verification of the Model. *Combustion, Explosion, and Shock Waves, 41(3),* 336-345.
11. Nigmatulin, R.I. (1987). *Dynamics of the multiphase media* (in Russian). Moscow, Nauka, Vol.1-2.
12. Dorodnitsyn, L.V. (2000). Acoustics in viscous subsonic flow models with nonreflecting boundary conditions. *Computational Mathematics and Modeling, 11(4),* 356-376.